

# Review of polarization components for infrared imaging systems: from wire-grid structured surfaces to reconfigurable metasurfaces

C. COTIRLAN SIMIONIUC<sup>a,\*</sup>, A. RIZEA<sup>b</sup>, C. MARIN<sup>c</sup>

<sup>a</sup>National Institute for Research and Development of Materials Physics, 405A Atomistilor Str., Magurele 077125, Ilfov, Romania

<sup>b</sup>ProOptica S.A., 67 Gh. Petrascu Str., Bucharest 031593, Romania

<sup>c</sup>Institute of Optoelectronics S.A., 67 Gh. Petrascu Str., Bucharest 031593, Romania

Infrared imaging polarimetry with structured surfaces components allows performance enhancement for observation, supervision, identification devices, generally far-field detection in low visibility conditions (night, fog, smog, haze, smoke, heavy rainfall, underwater conditions), for civil applications, e.g. environmental monitoring or communications, which aims to reduce the risk of traffic accidents, as well as defense and security purposes, where a tactical advantage is needed. Other applications aim at improving the performance of sub-wavelength imaging systems: spatial scanning, optical flaw detection, microscopies, medical tomography or cancer diagnostics systems, generally near-field range investigation. We review many important polarization components from wire-grid structured surfaces to reconfigurable metasurfaces, that can be achieved in order to manage sub-wavelength near-field details and their transfer in far-field by polarimetry techniques without moving parts. Advanced research is needed to show which concept will prevail in the market for the achievement of ultracompact polarization optical components and their integration into a functional model of polarization state analyzer for imaging systems with high efficiency in long wave infrared.

(Received October 6, 2017; accepted June 7, 2018)

*Keywords:* Image enhancement, Superresolution, Polarization-selective devices, Surfaces

## 1. Introduction

### A. Overview

An appropriate approach for easy removal of environmental effects caused by difficult visibility conditions (aerosols, rain, darkness) in passive acquisition of images is based on the fact that the natural light scattered by particles in atmosphere is partially polarized. The Rayleigh scattering (on gas molecules) and the Mie scattering (on aerosols) produce both polarization and depolarization of radiation. Generally, the polarization depends on the following features: the radiation source (spectrum, polarized or unpolarized emission, continuous or pulsed emission), the target object (if it is natural or artificial) and the environment particles (reflection, absorption, scattering, polarization characteristics). The photons that are coming from a disturbing environment are ballistic and snake. The first and the last have an unscattered path or slightly deviated route. They keep all polarization aspects of the source and also form the image. These photons are very few in number and only they should be allowed to pass through the "gate" to the detector. Sometimes special techniques are required for extraction and amplification. Noise generating phenomena are back-scattering and multiple scattering. Optical filtering can cancel the scattering effects only in particular

situations. Otherwise, it cannot cancel the effects of scattering. Even if the polarization is low, a physical spectral analysis can be made on a wide range of weather and visibility conditions.

Therefore, the imaging polarimetry operates in conditions far from ideal. The polarimetric approach does not rely on specific modeling of Rayleigh scattering, for example, nor on the knowledge of illumination directions, but only on images acquired through polarizers with different orientations. In many applications, polarization phenomena are ignored and scalar optical field is analyzed. While the scalar approach can be quite accurate in many situations, the ability to measure the polarization of light coming from an observed object provides additional details that can be exploited to improve the equipment performance. If the polarized light which is observed both entering and exiting the optical system is described by Stokes vectors, then in the generalized polarimetry, the analysis optical system will be described by fourth order Mueller matrix [1]:

$$[\text{Light output}] = [\text{Mueller Matrix}] \times [\text{Light entry}] \quad (1)$$

The components of the polarization Stokes vector are described by a matrix:

$$S = \begin{bmatrix} S_0 \\ S_1 \\ S_2 \\ S_3 \end{bmatrix} \propto \begin{bmatrix} I_0 + I_{90} \\ I_0 - I_{90} \\ I_{45} - I_{135} \\ I_L - I_R \end{bmatrix} \quad (2)$$

where:  $S_0$  is the total intensity of the light,  $S_1$  is the difference between horizontal (+1) and vertical (-1) polarization,  $S_2$  is the difference between linear 45°(+1) and linear 135°(-1) polarization, and  $S_3$  is the difference between right (+1) and left (-1) circular polarization. Sometimes a single polarization parameter is sufficient. However, for increased performance two, three, or even four components of the polarization Stokes vector can be used. There is a wide range of approaches in the literature for reconfiguration of metamaterial devices, including polarization surfaces, but only for certain wavelength bands. An early survey of the development of reconfigurable and tunable metamaterial technology as well as of valuable applications are shown in ref. [2].

## B. Polarization components

A significant opportunity arises from innovative ideas needed to solve spatio-temporal trade-offs related to the number of detected Stokes vector components and the complexity of optical analysis. The simplest system uses a single serial processing channel with rotating polarizer relative to the waveplate and a detector array [3]. The most complex approaches use four separate channels with parallel processing [1] by integrating four polarization state analyzers (PSA), each analyzer being composed of one micro birefringent waveplate and one micropolarizer, in a four-state subwavelength pixelated array [4] for snapshot imaging. The last system has the advantage of eliminating temporal fluctuations between adjacent pixels. However, this system introduces signal degradation due to the diffraction and interference effects between pixels. In passive techniques for IR broadband one-dimensional polarimetric imaging, the rotation of a single linear polarizer is used, for differential polarimetry two polarizers and two separate channels of analysis are being used. For three-dimensional polarimetry, up to four pairs of polarizers and waveplates are involved. The active imaging polarimetry techniques are: LIDAR techniques and techniques involving frequency selective surfaces (FSS). The polarimetric imaging rebuilds the image of an object after determination of the parameters that give the polarization state of the light for each pixel in the image. The polarimetric imaging method involves sophisticated calibration and verification procedures. The discrimination by two-dimensional polarimetry is widely applied for the scattering media and it was shown [5] that the distance up to the targets, which can be detected, increased by factors of 2 to 3. When the polarimetric imaging is used in quasi-passive systems, this technique can improve the penetration up to 5÷6 photon mean-free paths in random media. For time-gated imaging, the use of polarization discrimination allows penetration to more than 10 photon

mean-free paths and achieves an improvement in contrast and color correction [6]. Many artificial objects have surface structures more uniform than natural objects or the background such as soil, vegetation or trees. All of them emit thermal radiation that is partially polarized. By examining the polarization state of the IR radiation and the correlation between the roughness and the IR emissivity, the ability to see the artificial objects barely discriminated from the background random signals can be significantly improved and the reception of signals perturbed by environmental factors may be enhanced [7]. Published experimental results [8] indicate that the linear polarized light penetrates larger distances than circularly polarized light through biological tissues. Also, the visibility in fog, rain, smoke, mist or darkness is a major problem in aviation. Therefore, there are software that have allowed the detection of random weather events, identifying and monitoring their activity using polarimetric imaging techniques, such as a dual system: passive (IR) and active (LIDAR) [9]. By using a polarization discrimination technique the system is able to warn of the ice crystals. These are an environment with strong polarization. In phenomenological terms, the polarization signatures in the following regions: visible (VIS), 0.75÷1.4µm (NIR) and 1.4÷3 µm (SWIR) of the spectrum are dominated by reflectance and are dependent of external light sources, primarily the sun. In VIS, NIR and SWIR the polarization has a wide dynamic range and can provide a rapid spatial variation in imaging of external scenes depending on the time of day or location sensor. In the 3÷8 µm (MWIR) and 8÷15 µm (LWIR) ranges, the polarization signatures are a combination of reflected and emitted radiation, which tends to reduce the overall level of polarization [3].

In the 15÷1000 µm (FIR) range, the signatures are dominated by emissions and can be very stable over time. Unfortunately, in the LWIR and FIR the spatial resolution is reduced. Likewise, the cost and the complexity of the systems are generally high. In the case of outdoor measurements, the fastest variations of polarization versus wavelength derived from the spectral characteristics of the atmosphere [10]. Some problems may arise in LWIR and FIR, typically there the signal is weak and the resolution of sensor is low. The advantages would be that signatures are dominated by emission of target [1] and have less dynamic range in polarization. Thermal imaging in the 8÷12 µm range has a significant advantage due to thermal contrast which does not depend on the presence of an external source. Any object that is warmer or colder than the rest of the scene will have a thermal contrast. But the polarization properties of the emissive objects are more complicated. They do not depend only on the temperature of the target object and the surrounding objects, but also on that of the background objects, even if they do not appear in the scene and these strongly affect the measured polarization signature [3]. The polarizers can be birefringent crystals (e.g. calcite), dichroic elements and reflection or transmission polarizers with thin layer of metal elongated particles or linear reticules. In NIR and SWIR, polarizers with thin layer of metal particles or wire-grid are more efficient than dichroic polarizers, offering

$10^5:1$  contrast [11]. For the polarization control in MWIR÷LWIR, besides metallic wire-grid polarizers, there aren't any efficient and compact polarization components commercially available. The current polarizers are made of metal grid deposited on transparent substrate with low refractive index in MWIR÷LWIR. Because the degree of polarization of IR radiation depends weakly on the wavelength and the angle of incidence, they are used in broad band applications. The waveplates are obtained on an IR transparent substrate with high refractive index. The achromaticity is commonly provided by a serial arrangement of two crystal slabs of  $0.5\div 0.9$  mm thickness with different dispersions, ensuring a little and constant phase difference between the states of polarization in a certain spectral range. However, the achromaticity of the retarders can be obtained by form-birefringent option, i.e. the surface is structured as a diffraction grating by the etching of a dielectric substrate in order to insure a spatial period below the lower limit of the spectral range [4]. An antireflection (AR) coating carefully made on the phase retarder surface without nano- or microstructure, with a thickness not exceeding the distance between the lines of the structure, reduces the variation of extinction ratio amongst the polarization components in the MWIR. Achieving the AR coatings on nano- or microstructured surfaces is not feasible, because the coverage would change the optical characteristics of the network. In addition, the deposition rates cannot be controlled on the vertical walls of nano/ microstructure or AR coating thickness may be greater than the width of the spaces between the metal lines of the network [4]. The operation principle of the metal grids as IR polarizers is based on a strong anisotropic absorption of light in metallic structure with sub-wavelength thickness of the grid line.

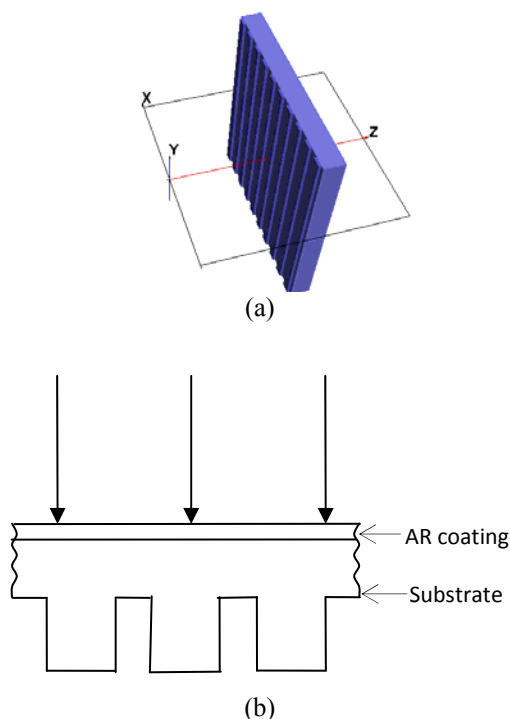


Fig. 1. (a) Wire-grid linear polarizer [12], (b) Ronchi profile for birefringent retarder or quarter waveplate

For the MWIR range, the thickness of the metal grid lines may be in the order of 200 nm [4].

A very good achromatic characteristic compared to the birefringent crystal can be obtained if in order to manufacture a physically large QWP, the form-birefringent option is chosen over the more traditional methods. The  $8\div 12$   $\mu\text{m}$  polarizers can be achieved with aluminum (Al) parallel lines with a period of  $1.4\div 2.0$   $\mu\text{m}$ , height of  $1.8\div 2.8$   $\mu\text{m}$  and with  $50\% \div 90\%$  duty cycle of the grating on Ge substrate ( $n\sim 4.0$ ) [13] (Fig. 1(a)). Classically, birefringent retarders can be made with Ronchi profiles etched directly on IR transparent substrate (Fig. 1(b)).

## 2. State of the art in the field

In order to exploit the advantages of modern technologies in the development and integration of the polarization components, such as achromatic broadband, ultracompact waveplates and linear polarizers, it is necessary to consider the metamaterials (MTMs) option, particularly metasurfaces (MTS). MTMs can be described as a class of artificial composite materials with engineered electromagnetic response, such as dielectrics with metallic inclusions or inductive structures smaller than the wavelength. These inclusions or are regularly distributed in the bulk of a dielectric as metaatoms. MTS are surfaces formed by a single layer of subwavelength MTM and control the phase of light in a highly localized fashion. MTM is projected to have a negative refractive index or dielectric constant  $\epsilon$ , and/or negative values magnetic permeability  $\mu$  [14, 15, 16]. The main features of a MTM are related to the ability to guide/control the light through its interaction with inclusions [17, 18]. The MTMs made using nanotechnology can be seen as "continuous effective" materials. Unlike a conventional insulating material, the material with negative refractive index considerably deviates the light, so it is enough to produce a superlens, for example, using of a thin plate of this kind of material with parallel faces (without curvature). In addition, the use of a material with negative refractive index leads to optical instruments without limitations related to the diffraction. The difficulties encountered in the development of technologies for MTM are special, because obtaining negative refractive index requires a nanoscale combination between materials with special electrical and magnetic properties. The negative refractive index strongly depends on the wavelength of the used radiation. For example, the effect ( $n<0$ ) may occur for red light but it is not observed for blue light. The MTMs have already demonstrated their capabilities in radio, microwave (THz), IR, VIS and UV fields. The ultracompact waveplates were designed and simulated with thicknesses lower than operating wavelength using MTM with a remarkable anisotropy [19]. These waveplates are more efficient in the visible spectrum than the conventional wave retarders commercially available. The birefringent MTM and perfect lenses [20] are new components with unusual properties, and more

importantly, could show a wider range of potential applications in comparison with isotropic MTM and perfect lenses described by Veselago [14] and Pendry [15], that have generated the idea of taking advantage of superlenses for evanescent waves processing. The W. Lukosz's older demonstration [21], which proves that it is possible to increase the bandwidth of the harmonics that form an image by redirecting spatial frequencies, even doubling bandwidth by transmitting only optical information for one state of polarization, is fully applicable to the ultracompact polarization components. Creating a MTM to ensure operation on a wider range of wavelengths, such as the  $8\div 12\ \mu\text{m}$  domain, remains a challenge. But the most interesting phenomenon observed in MTMs is a giant improvement of the electric field of the light at plasmonic (metallic) grid surfaces or nanostructured MTS. This improvement occurs only for the first order of diffraction of a single polarization state (p). However, looking for the best plasmonic properties, few metallic materials were found, but with high mobility carriers [22, 23]. The propagation of the light just through a thin layer of silver, called near-field superlens (NFL), has been experimentally studied since 2005. Thus, the evanescent waves are amplified in the thin metal layer and contribute to image formation in near field. If over the metal layer is performed a metallic diffraction grating or the NFL has a curvature radius [24], then this structure converts evanescent waves into propagating waves, and an image with resolution beyond the diffraction limit in the far field is obtained [18]. Amplification of the electric field may be higher than for usual schemes [25, 26] for surface-enhanced Raman scattering and, what is most important, it refers to the entire surface. The nanostructured MTS are not less important than bulk metamaterials and deserve creating a special theory [27] for them. Sometimes, the difference from a homogeneous material is small enough to justify the definition of effective refractive index. However, many nanostructured MTS cannot be characterized by specific parameters of the bulk material. This assertion applies to structures with spatial dispersion effects. In these cases the models based on homogeneity should be different from those based on spatial mediation in volume and once a parameter is found, although it would be called effective, it will not give any useful information to characterize the MTM [51, 54]. Fabrication of QWP or polarization splitter using anisotropic MTM is based on the fact that variations in the amplitude and the phase of electromagnetic radiation are interrelated. At frequencies where the phase variation is maximum, the amplitude remains almost unchanged and vice versa [28]. Artificial grid structures have been reported [29]. Most of the structures with micrometer or submicrometer period for the MWIR polarizers or filters are obtained by structuring of thin metal layers evaporated on IR transparent polymers or crystals ( $\text{CaF}_2$ , KRS5, etc.) using lithographic methods [30]. The design of such a wire-grid polarizer by analogy with a transmission line taking into account the effect of different support substrates, the method for obtaining such a polarizer by lithographic techniques and measurements in the range from  $20\ \mu\text{m}$  to

hundreds of microns for the obtained device are shown in ref. [31]. Its performance [32] compares favorably with those of the polarizers obtained by other experimental methods using an assembly presented in Fig. 2.

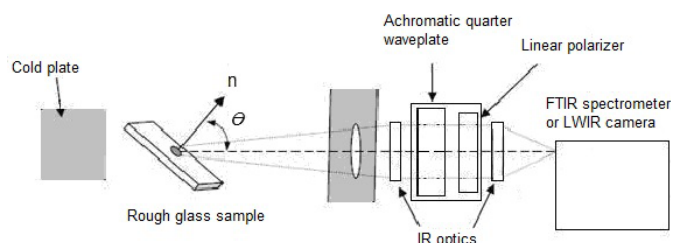


Fig. 2. The application for spectral and polarimetric measurements (FTIR spectrometer, respectively LWIR camera) for evaluating the surface roughness (adapted from K. P. Gurton et al. [7]). The QWP and the LP form a PSA. Auxiliary IR optics is a focus subsystem. FTIR is the main method for the characterization of thin MTM or a MTS

In conventional bulk optics, circular polarization is analyzed using a QWP in combination with a LP, *i.e.* PSA. The diagram from Fig. 2 can be used to measure the Stokes vector components, if the sample is a Frequency Selective Surface (FSS) excited by a thermal source [3].

Polarization broadband optics is suitable for analysis instruments such as a LWIR camera for evaluation of Stokes vector components or a FTIR spectrometer. FSS can be used for calibration and IR target simulation [33, 34]. Typically, their period is comparable to the wavelength of the work radiation. FSS can be designed to be sensitive or insensitive to IR polarization [35]. A temperature of  $45^\circ\text{C}$  is sufficient to excite the FSS and obtain thermal image with a LWIR camera through polarization optics [36]. Polarimetric estimation requires multiple measurements made in different optical conditions for each observed scene. This measurement strategy makes the evaluated polarization to be susceptible to errors. Sources of errors depend on the type of measurement scheme used. With scheme designed for  $8.3\div 9.3\ \mu\text{m}$  range [37], an analytical model is used for realistic interpretation of the results obtained by simultaneous measurements of the scene polarimetric modulated. The model is radiometrically corrected and takes into account the temperature of system optics, spatial unevenness and drift, optical resolution and other noise sources.

This model can be used in our simulations to validate the laboratory measurements and to determine the precision and accuracy of the system. Imaging systems using linear polarization microcomponents have been demonstrated from VIS [38, 39] to LWIR [30]. However, these systems have examined only linear polarization components of the Stokes vector, due to the difficulty of fabricating microstructures sensitive to circular polarization.

Several alternative approaches to manufacture waveplates were reported [40, 41, 42, 43]. The

birefringence has been reported in a type of asymmetric plasmonic analog antenna structures (Fig. 3) including meanderline [44], matrices of holes [45], cross-shaped antennas [46] and elliptical antennas [47] or networks of spirals with a central opening [48].

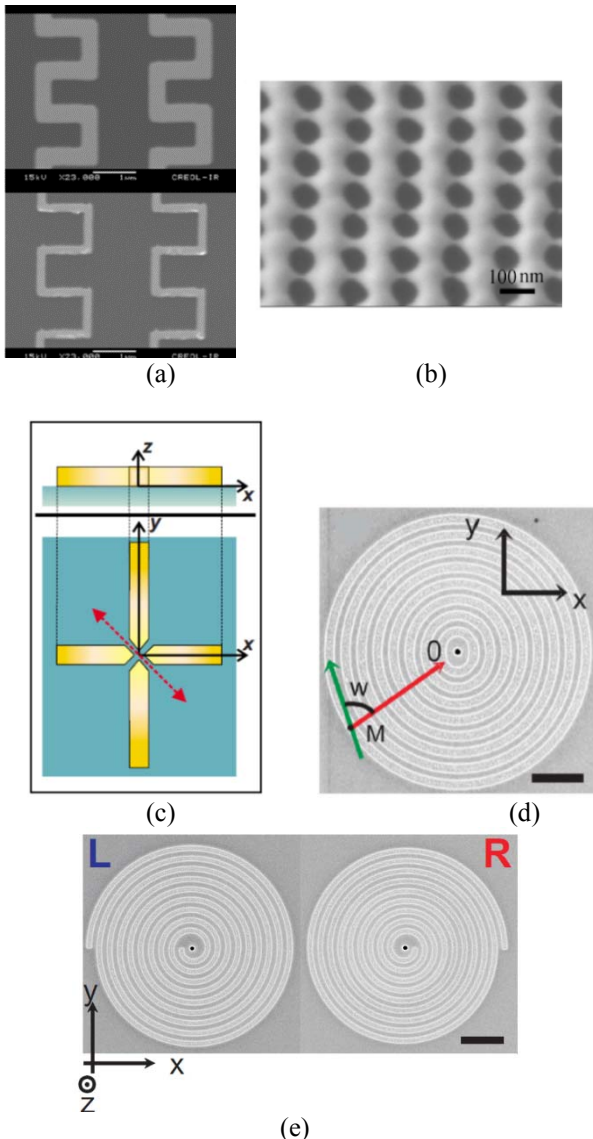


Fig. 3. Several approaches for waveplate MTM configurations: (a) © 2010 OSA [44], (b) ©2010 AIP [45], (c) © 2009 B.Hecht [46], (d) © 2008 A. Drezet [47], (e) © 2008 OSA [48]

The liquid crystals integrated with wire-grid polarizers provide a possible approach to obtain a circular polarization signature in imaging applications [49]. It has been shown that a gold-type MTM with three-dimensional spirals area operates as a circular polarization filter in the IR spectral range ( $3.5\div 7.5\mu\text{m}$ ) [50].

An example of MTM with controlled birefringence in far IR range involves elementary cells with metallic (gold) cross structures with arms of  $200\mu\text{m}$  and a thickness of  $25\mu\text{m}$ . Due to inevitable dispersion that occurs in transmission bands, characteristic to the two arms of the

cross structure, the resulting MTM has different values for the effective refractive index for the two polarizations and, thus, a plate from this MTM acts as a birefringent material. The length of the horizontal cross arm varies in order to introduce the tunability of system birefringence [51].

Due to the large refractive index contrast achievable in such proposed structures, the total thickness of the retarder plate is less than the thickness of a quarter-wave plate based on liquid crystal operating in the range of THz [52]. Manufacture of optical MTM with negative refractive index is quite problematic, due to the obtaining requirements for structural units or "metaatoms" with dimensions of  $100\text{ nm}$  or below  $100\text{ nm}$ , and an arrangement period of  $300\text{ nm}$  or less. The need for higher resolution for the VIS range makes the Electron Beam Lithography (EBL) to be still the first choice in manufacturing small area MTM ( $100\mu\text{m} \times 100\mu\text{m}$ ). Larger areas require longer imprinting time and, therefore, increase the cost of implementation. A serial technology similar to EBL technology, widely used for rapid prototyping, is the Focused Ion Beam (FIB) milling. However, FIB is not considered to be feasible for large-scale manufacture of MTM for practical applications due to the low productivity.

Another approach to manufacture high-quality large-area ( $\text{cm}^2$ ) MTM is the Interferential Lithography (IL). To increase the resolution the IL can be combined with self-assembling techniques. Moreover, this technique could also be applied in the manufacture of three-dimensional (3D) MTM by overlapping two-dimensional layers in 3D structures. This step of arrangement of 2D layers obtained with IL into 3D stack was not done until now due to the complexity of multiple alignments. Nanoimprint Lithography (NIL) is another promising technological approach to create large scale high quality MTM. The NIL is a parallel process and has the advantage of high productivity, high resolution and low cost [58]. Because the NIL requires a stamp made by other nanotechnology (such as EBL) it is ideal for parallel production of already optimized MTM, when preliminary test structures were patterned by EBL.

The first steps towards the realization of 3D MTM were made both by direct creation of multilayer structures (instead of a single functional layer) and by using the layer-by-layer technique. Both approaches to produce stacking MTM have limitations, namely the problem of challenging lift-off procedure in the first case and alignment requirements in the second case. While complex 3D nanostructures can be fabricated via several techniques (e.g. direct electron beam writing, FIB or chemical vapor deposition), these methods are too complex and time-consuming to be adapted to large-scale production of MTM. A manufacturing method for 3D MTM that is widely regarded today as one of the most promising approach is based on two-photon-photopolymerization (TPP). This technique provides resolution at the diffraction limit ( $\sim 100\text{ nm}$ ) and due to the inherently nonlinear multiphotonic process, it shows 3D capability. Unlike direct writing of complex structures in the polymer matrix with a single laser beam, the large-scale 3D polymer

structures for future practical applications can be achieved through TPP technique. 3D multilayered, polymer-metal structures [53, 54] can also be made by NIL. This method provides high reproducibility over large areas of the order of  $\text{mm}^2$ . Combined with multiple material deposition technique, these lithographic approaches could be adapted for future MTM configurations. Careful selection of materials, *e.g.* new crystalline metal structures with lower absorption (instead of the traditional silver and gold) or less metallic compounds, together with the optimization of the manufacturing process for low roughness and high uniformity, can lead to the creation of low-loss optical MTM on a substrate with high thermal stability.

Ultrathin MTS made of novel low-loss plasmonic material components is a promising way to address this challenge. Researchers can work to replace silver and gold in materials that are created either by making semiconductors more metallic by adding metal impurities to them, or by adding non-metallic elements to metals, thus making them less metallic. Examples of new materials include transparent conducting oxides (TCO) [55], titanium nitride and graphene [56].

Another possibility is to introduce a material with optical gain to compensate the losses in MTM. Even though it is still a long way to becoming reality, 3D MTM with negative refractive index at optical frequencies of interest, several technological approaches seem to be feasible [57]. With technologies like NIL, contact lithography, direct laser engraving and new types of self-assembly, 3D MTM can be created with structural units smaller than the wavelength [58] for superlenses (Fig. 4).

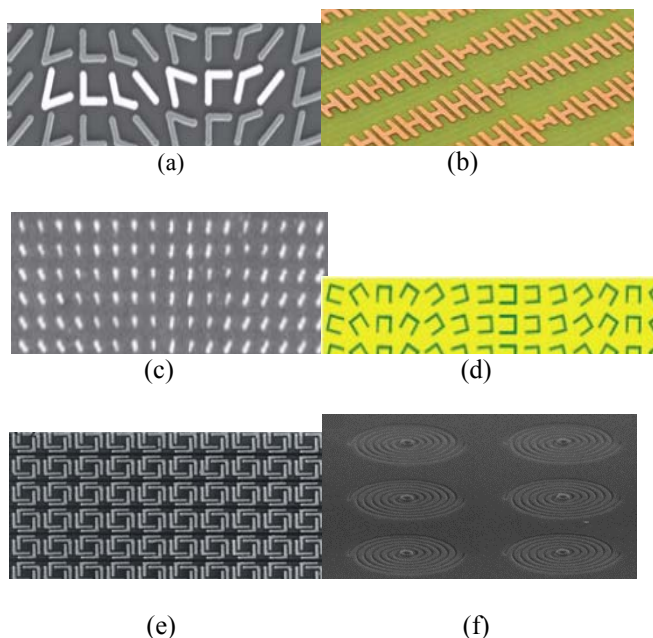


Fig. 4. Periods of conductive elements or plasmonic antennas with fixed forms on superlens MTS: (a) © 2014 F. Capasso [59], (b) © 2012 L. Zhou [60], (c) © 2012 T. Zentgraf [61], (d) © 2012 OSA [62], (e) © 2007 AIP [63], or circular polarizers: (f) © 2012 OSA [64]

Thus, a selection of future manufacturing techniques requires a reliance on considerations of structural quality built with the methods suggested above and lower associated costs.

The MTM characterization was described in a synthesis article [27]. The error correction strategies were defined and modeled for a conventional system in ref. [65]. IR polarizers and superlenses made from MTM give the following advantages: there are no optical aberrations, the optical substrate is not required [30] and they can collect more diffraction orders for improved contrast.

### 3. Future directions: reconfigurable photonic metasurfaces

A special interest in MTS as new kind of 2D MTMs was developed since 2011 to achieve exotic optical phenomena and optical components, including negative refraction or reflection, plasmonics, polarization, as well as aberration-free ultrathin lenses [66, 67]. The evolution of MTS is shown in Fig. 5 on the basis of Gartner's hype cycle. *E.g.* surfacetrionics (SFX) is a new research area that concerns the conception, analysis and realization of reconfigurable, sensorial, adaptive and cognitive "skins" for sensing and communications [68]. Various technologies are emerging to provide modulation of MTS responses using mechanical, electrical, or optical control. Therefore, unconventional devices without volumetric counterparts, but with reduced dimensions can be achievable. Nanoarchitectronics (NTX) is a scientific jargon term developed in a document written by the 40 members of the FORESEEN consortium as a roadmap for a next generation of nanostructured MTS as artificial and bio-inspired "skins", able to adapt themselves to the environment, being cognitive and reconfigurable as well. SFX is aimed at combining radiating and sensing functions for future communication beyond 5G, namely antennas, radars, and body area networks. Furthermore, various technologies are nowadays emerging to provide modulation of MTS response using mechanical, electrical, or optical control. Although the general purpose of these approaches is to obtain tunable versions of static MTS, recent studies have uncovered that the impact of dynamic MTS far exceeds tunability alone and comprises new physical effects such as Lorentz non-reciprocity. The FORESEEN document denotes all the area of dynamic MTS to achieve time-varying properties and their conceivable applications as "Surfacetrionics". SFX can be divided in "phase variable SFX" and "sensing/radiating SFX". Phase variable SFX can control and address the surface/plasmonic waves as: phase gradient changing SFX by stretching or heating, phase gradient changing by light-surface interaction, phase gradient changing fluid based SFX, phase gradient changing SFX by micro- or nano-mechanical actuations, Huygens type SFX, dispersion SFX (for surface/plasmonic wave control), transformation optics SFX, subwavelength focusing lenses, non-reciprocal and time reversal lenses. On the other hand, sensing/radiating SFX receive (RX)/transmit (TX) signals

or power in free space as leaky-wave SFX, RX distributed conformal surfaces, adaptable and stretchable receiving surfaces, variable radiating apertures, energy harvesting SFX, cloaking SFX [68]. In the U.S., the Multidisciplinary

University Research Initiative (MURI) “Active Metasurface for Advanced Wavefront Engineering and Waveguiding” has been launched in 2014 with support of AFOSR (Air Force Office for Science and Research) [69].

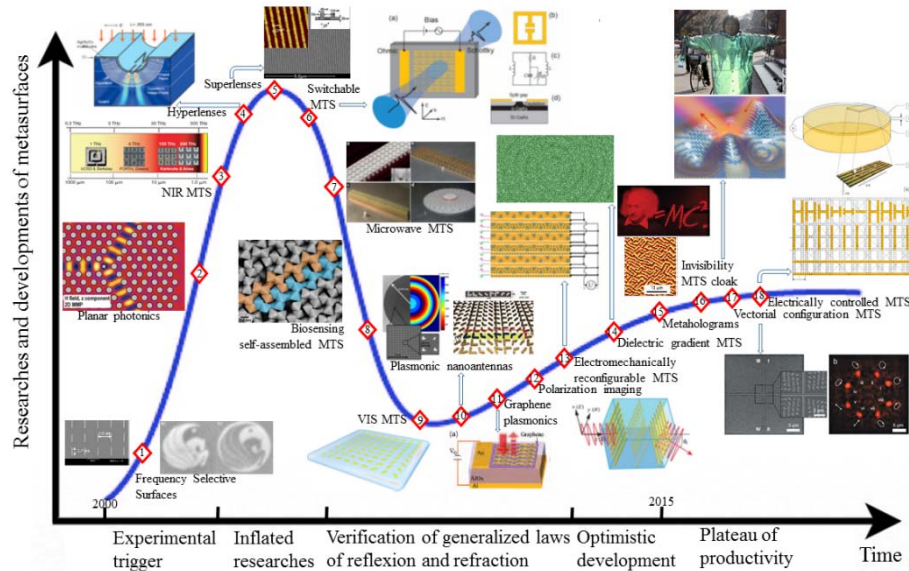


Fig. 5. The evolution of MTS in agreement with the general Gartner's hype cycle for emerging technologies [70]: <1>©2002 OSA [33], <2>©2005 K. Rauscher [71], <3>©2006 C. M. Soukoulis [72], <4>©2007 AAAS [73], <5>©2007 OSA [74], <6>©2007 R. Averitt [75], <7>©2008 OSA [76], © 2008 OSA [77], ©2009 AIP [78], <8>©2011 J. Henzie [79], <9>©2012 X. Chen [80], <10>©2012 ACS [81], © 2012 X. Ni [82], <11>©2013 ACS [83], <12>©2013 AAAS [84], <13>©2013 J. Y. Ou [85], <14>©2014 AAAS [86], <15>©2015 G. Zheng [87], <16> © 2003 S. Tachi [88], ©2015 AAAS [89], <17>©2015 L. Li [92], <18>©2015 NIMP[90]

This project involves: Harvard University (leader), Columbia University, Purdue University, Stanford University and University of Pennsylvania. It explores the underlying physics with focus on the connection between active MTS design, the control of SPP and reflected/transmitted beams, and on the interaction of device building blocks (optical antennas, dielectric resonators, quantum emitters, etc.) including nonlinear MTS for broadband frequency conversion. The MURI project has many affinities with a portion of the NTX Initiative.

Also, J. Valente *et al.* have demonstrated that spatial arrangement and optical properties of MTM nanostructures can be dynamically controlled using currents and magnetic fields [91]. Another initiative was included in a H2020 project from National Institute of Research and Development of Materials Physics (NIMP), “New type of flat optics with electrically controlled optical properties by surface structure based on low-loss plasmonic materials”, for development of aberration-free, ultrathin plasmonic optics with voltage-controlled properties, Fig. 6.

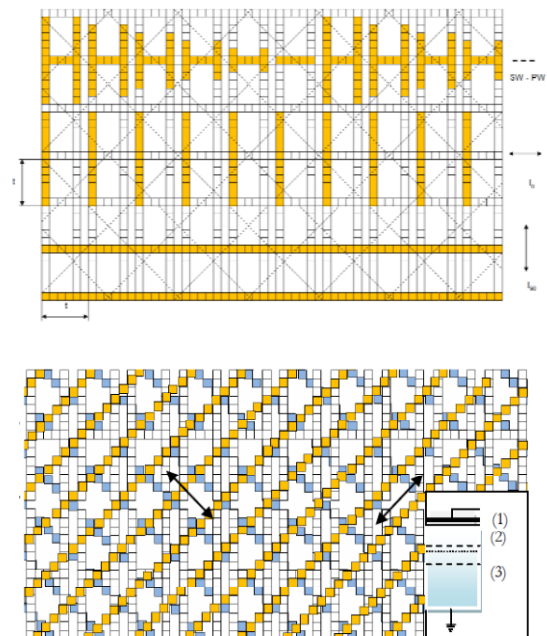


Fig. 6. Electrically configurable MTS based on Schottky array architecture concept: (left side) for EW (SW) to PW conversion and two dimensional imaging polarimetry, and (right side) only two dimensional imaging polarimetry (inset with detail of Schottky pixel structure for conduction switching: (1) IR-TCO layer, (2) P-TCO layer, (3) quartz or Si substrat)

Recently, metallic or less metallic nanostructures with a very limited sample thickness offer efficient solutions in polarization control with a vectorial configuration of surface plasmon field. In most of these devices, the functions were usually limited to a few polarization states. Lin Li *et al.* presented a plasmonic polarization generator that can reconfigure an input polarization to all types of polarization states simultaneously.

The plasmonic polarization generator is based on the interference of the in-plane field of the surface plasmons. This longitudinal field gives rise to versatile near-field polarization states on a metal surface. The in-plane field of surface plasmon-polaritons (SPPs) with proper polarization states and phases can be selectively scattered out with a well-designed nanohole array in order to obtain the desired light beams.

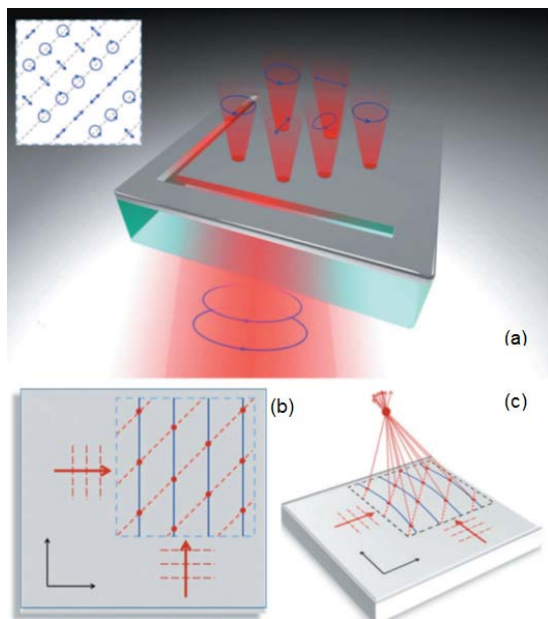


Fig. 7. (a) Schematic of the polarization reconfiguration process. The inset is the polarization states of the in-plane SPP field distribution with incident RCP light. Design strategy for routing the polarization states to special beams: plane wave scattering (b) and focusing beam scattering (c) © 2015 T. Li [92]

A manifestation of eight focusing beams with well-routed polarizations, represented in Fig. 7, was experimentally demonstrated [92]. For near-field applications, such as microscopy or imaging analysis, the superlenses can be characterized by the smallest resolvable distance given by  $\Delta r = \lambda/2n\sin(\theta)$ , where  $\lambda$  is the working wavelength in free space,  $n$  is the refractive index of the surrounding medium, and  $\theta$  is the collection angle of the imaging optics. To overcome the diffraction limit and achieve nanoscale optical imaging, a straight-forward way is to detect the signal in the near-field of the object [93].

For far-field application as imaging polarimetry, the polarization components from a PSA should be evaluated with a factor of merit which combines the great

transmission efficiency (TE) with the great extinction ratio (ER), as product  $TE \times ER$  versus wavelength [94].

#### 4. Conclusions and outlook on real world applications

Many fish, cephalopods, crustaceans, insects and other animals are able to perceive polarized light. Some of the current applications that are mimicking the visual behavior of the animals are: object recognition by segmenting of scene and disclosure of camouflage, communication and underwater viewing. An approach to underwater vision with processing algorithms on computer, which removes the degradation effects of underwater images with natural light, is shown in ref. [95]. Through a physical analysis of images obtained by polarizers and 3D rendering from different angles, the natural backscattering is associated to the partial polarization of light. The used algorithm reverses imaging process and leads to better visibility compared to previous methods. Also, there are applications that utilize polarization and their inspiration is not biological, such as calibration of cameras, microscopy [96], fiber optic communications, industrial control, robotics [97].

Near field superlenses exploit details from evanescent waves and surface waves to lower resolution below diffraction limit, whereas polarization components for near field (Fig. 8) or far field (Fig. 9), *i.e.* linear polarizer and QWP, use Stokes vector components in order to improve sharpness, transparency and contrast.

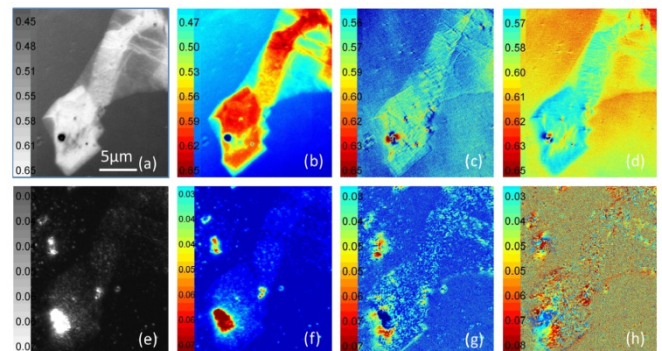


Fig. 8. Near field imaging polarimetry: bright (a to d) and dark (e to f) field images taken by the modulated polarization parameter imaging system using 100x objective, direct grey scale image of a chemically prepared graphene overlapped to 1 to 6 layers on a glass slide (a, e), its indirect polarization parameter images of polarization averaged intensity  $I_{dp}$  (b, f), polarization phase difference (c, g) and polarization angle of slow axis  $\Pi$  to horizontal axis (d, h), © 2014 OSA [98]

Phase difference contrast image (Fig. 8(g)) resulted from collecting phase changes during polarization scan contains stronger image contrast. With even higher sensitivity than phase difference to anisotropic field variation, polarization angle contrast picked up more near field scattering spectra to form the image (Fig. 8(h)) filled

with characteristic scattering noise. However, this is highly desirable for scattering modeling and edge characterization.

On the automotive market, the FLIR PathFindIR II and MICRO T-SCAN imagers are available [99]. These systems distinguish objects below 310 meters without polarization accessories, but with accessories the system could view from 2 times (differential polarimetry) to 10 times more (polarimetry with temporal integration), a sufficient distance for braking and collision avoidance with unmarked road users under difficult visibility conditions.

Also, a three-dimensional image can be obtained combining the Stokes images with Fresnel relations to extract the surface normal at each pixel, and integrating over these surface normals [100].

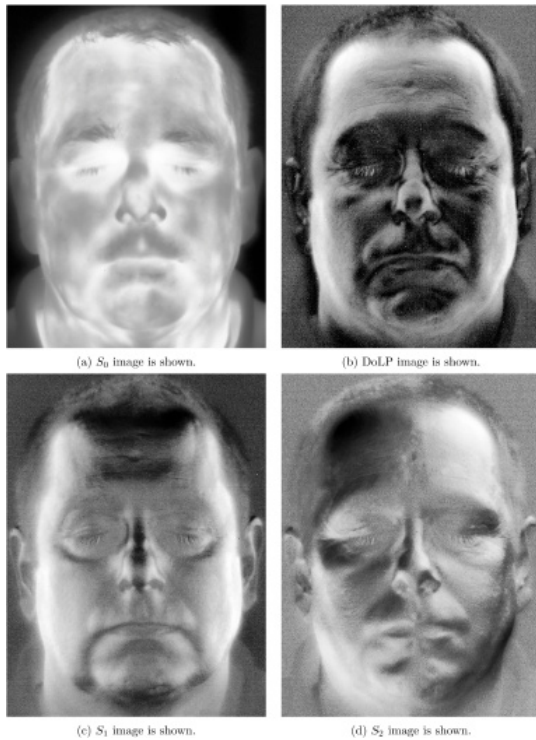


Fig. 9. Optical details revealed by far-field imaging polarimetry, © 2014 OSA [100]

In molecular spectroscopy, the  $\lambda = 3\div 10 \mu\text{m}$  range is of great interest. One of the main uses of the IR polarizer is monitoring the molecular orientation in thin films and fibers. During the obtaining process, the polymers tend to be oriented along the axis of mechanical tension and the preferred orientation is preserved after ceasing the phase flowing. In some cases the polymers are a mixture of material phases: crystalline (polarized) and amorphous (less polarized). To study the orientation, the polarized light is directed on film or fibers. If the electric vector of polarized light coincide with the orientation of the active dipole in IR, then the absorption increases, thus the absorption band and the molecular group orientation are easily identified [101].

A biosensor based on bimetallic nanoparticles attached to electrodes that are more sensitive and can give a faster response to polluting factors is emerging through a collaboration between NIMP and Institute of Physical Chemistry (IPC) under program PCCA-1/2011. A new biosensor for detection of Localized Surface Plasmon Resonance (LSPR) displacements in VIS can be developed with the same type of bimetallic nanoparticles (Pt-M, Pd-M, Rh-M, with  $M = \text{Cu, Ag and Au}$ ) fixed on a dielectric surface where total internal reflection of laser beam occurs.

The dielectric and the included bimetallic nanoparticles are a specific MTM for application in molecular biodetection. Future studies are required in order to assess if these bimetallic nanoparticles arranged in strips or parallel lines on LWIR transparent substrate will effectively polarize the radiation [102].

In addition to increase the visibility for canceling the navigation hazards in aviation, automotive and navy, experimental results are published [103] to indicate that the linearly polarized light travels longer distances through biological tissues than the circularly polarized light. This is the premises of developing rapid diagnosis polarimetric noninvasive methods in cancerous tumors using medical thermal system or multispectral imaging Mueller polarimeters. Now, the proposed polarimeters for diagnosis operate in the visible spectral range [104]. In order to make early detection of cancer, to improve the performance of the biopsy by exact location of the cancer cells, to specify the tumor stage before surgery, to detect residual tumors after treatment and monitor the recurrence of tumor, the spectral range should be extended. For cavities of the human body, in order to increase contrast, the polarimetric investigation can be done using a fiber optic with illumination in detected spectral region. Depending on the type of aerosols in the atmosphere the polarization degree of thermal radiation varies. In environmental pollution monitoring, a direct application of a system with IR PSA follows the warning when the radiation transmission falls below a certain limit due to increased environmental pollution [105].

Using optical MTS or MTM, the superlenses and polarization components can be further developed. Then, new materials and devices with special properties, new technologies [106] and procedures will be developed following research and experiments.

### Acknowledgements

This work was supported by PN II UEFISCDI no. 277/2014 and Core Program 2017.

### References

- [1] J. S. Tyo, Dennis L. Goldstein, David B. Chenault, Joseph A. Shaw, *Appl. Opt.* **45**, 5453 (2006).
- [2] J. P. Turpin, J. A. Bossard, K. L. Morgan, D. H. Werner, P. L. Werner, *Int. J. Antenn. Propag.* **2014**,

- 429837 (2014).
- [3] J. S. Tyo, Bradley M. Ratliff, James K. Boger, Wiley T. Black, David L. Bowers, Matthew P. Fetrow, *Opt. Express* **15**, 15161 (2007).
- [4] S. A. Kemme, A. A. Cruz-Cabrera, R. R. Boye, T. Carter, S. Samora, C. Alford, J. R. Wendt, G. A. Vawter, J. L. Smith, Sandia National Laboratory, SAND2006-6889 (2006).
- [5] J. S. Tyo, M. P. Rowe, E. N. Pugh, Jr., N. Engheta, *Appl. Opt.* **35**, 1855 (1996).
- [6] Y. Y. Schechner, S. G. Narasimhan, S. K. Nayar, *Appl. Opt.* **42**, 511 (2003).
- [7] K. P. Gurton, R. Dahmani, G. Videen, Army Research Laboratory, ARL-TR-3240 (2004).
- [8] V. Sankaran, M. J. Everett, D. J. Maitland, J. T. Walsh, Jr., *Opt. Lett.* **24**, 1044 (1999).
- [9] R. Billmers, Topic: 06-1 A1.06-9659, <http://www.rlassociatesinc.com>.
- [10] C.C. Chen, Report R-1694-PR (1975).
- [11] Melles Griot, "The practical application of light" Technical Guide (2014).
- [12] C. Cotirlan-Simioniu, C. Logofatu, G. Iordache, A. Rizea, D. V. Ursu, *J. Optoelectron. Adv. M.* **18**(11-12), 922 (2016).
- [13] M. W. Kudenov, E. L. Dereniak, L. Pezzaniti, G. R. Gerhart, *Proc. SPIE* **6972**, 69720K (2008).
- [14] V. G. Veselago, *Sov. Phys. Usp.* **10**, 509 (1968).
- [15] J. B. Pendry, A. J. Holden, D. J. Robbins, W. J. Stewart, *IEEE Trans. Microwave Theory Tech.* **47**, 2075 (1999).
- [16] D. Lu, Z. Liu, *Nat. Commun.* **3**, 1205 (2012).
- [17] S. Durant, Z. Liu, J. M. Steele, X. Zhang, *J. Opt. Soc. Am. B* **23**, 2383 (2006).
- [18] Y. Xiong, Z. Liu, S. Durant, H. Lee, C. Sun, X. Zhang, *Opt. Express* **15**, 7095 (2007).
- [19] M. Iwanaga, *Appl. Phys. Lett.* **92**, 153102 (2008).
- [20] A. A. Zharov, N. A. Zharova, R. E. Noskov, I. V. Shadrivov, Y. S. Kivshar, *New J. Phys.* **7**, 220 (2005).
- [21] W. Lukosz, *J. Opt. Soc. Am.* **57**, 932 (1967).
- [22] G. V. Naik, V. M. Shalaev, A. Boltasseva, *Adv. Mater.* **25**, 3264 (2013).
- [23] J. Gao, K. Kempa, M. Giersig, E. M. Akinoglu, B. Han, R. Li, *Adv. Phys.*, **65**, 553, (2016).
- [24] I. I. Smolyaninov, Y.-J. Hung, C. C. Davis, *Science* **315**, 1699 (2007).
- [25] S. R. Emory, S. Nie, *Science* **275**, 1102 (1997).
- [26] F. J. Adrian, *Chem. Phys. Lett.* **78**, 45 (1981).
- [27] C. R. Simovski, *J. Opt.* **13**, 013001 (2011).
- [28] X. G. Peralta, E. Smirnova, A. K. Azad, H.T. Chen, A. J. Taylor, I. Brener, J. F. O'Hara, *Opt. Express* **17**, 773 (2009).
- [29] J. B. Pendry, A. J. Holden, W. J. Stewart, I. Youngs, *Phys. Rev. Lett.* **76**, 4773 (1996).
- [30] F. Mattioli, M. Ortolani, S. Lupi, O. Limaj, R. Leoni, *Appl. Phys. A* **103**, 627 (2011).
- [31] J. P. Auton, *Appl. Opt.* **6**, 1023 (1967).
- [32] M. A. El-Aasser, S. A. Mahmoud, *Optoelectron. Adv. Mat.* **11** (7-8), 398 (2017).
- [33] I. Puscasu, W. Schaich, G. D. Boreman, *Infrared Phys. Technol.* **43**, 101 (2002).
- [34] J. Ginn, D. Shelton, P. Krenz, B. Lail, G. Boreman, *Opt. Express* **18**, 4557 (2010).
- [35] J. S. Tharp, B. A. Lail, B. A. Munk, G. D. Boreman, *IEEE Trans. Antenn. Propag.* **55**, 2983 (2007).
- [36] S. L. Wadsworth, P. G. Clem, E. D. Branson, G. D. Boreman, *Opt. Mater. Express* **1**, 466 (2011).
- [37] J. K. Boger, J. S. Tyo, B. M. Ratliff, M. P. Fetrow, W. T. Black, R. Kumar, *Proc. SPIE* **5888**, 58880U (2005).
- [38] V. Gruev, J. Van der Spiegel, N. Engheta, *Opt. Express* **18**, 19292 (2010).
- [39] V. Gruev, R. Perkins, T. York, *Opt. Express* **18**, 19087 (2010).
- [40] B. Päivänranta, N. Passilly, J. Pietarinen, P. Laakkonen, M. Kuittinen, J. Tervo, *Opt. Express* **16**, 16334 (2008).
- [41] Y. Pang, R. Gordon, *Opt. Express* **17**, 2871 (2009).
- [42] M. R. Shcherbakov, M. I. Dobynde, T. V. Dolgova, D. P. Tsai, A. A. Feyanin, *Phys. Rev. B* **82**, 193402 (2010).
- [43] A. C. Van Popta, J. Cheng, J. C. Sit, M. J. Brett, *J. Appl. Phys.* **102**, 013517 (2007).
- [44] S. L. Wadsworth, G. D. Boreman, *Opt. Express* **18**, 13345 (2010).
- [45] L. Feng, Z. Liu, V. Lomakin, Y. Fainman, *Appl. Phys. Lett.* **96**, 041112 (2010).
- [46] P. Biagioni, M. Savoini, J.-S. Huang, L. Duò, M. Finazzi, B. Hecht, *Phys. Rev. B* **80**, 153409 (2009).
- [47] A. Drezet, C. Genet, T. W. Ebbesen, *Phys. Rev. Lett.* **101**, 043902 (2008).
- [48] A. Drezet, C. Genet, J.-Y. Laluet, T. W. Ebbesen, *Opt. Express* **16**, 12559 (2008).
- [49] Z. Zhao, A. Bermak, F. Boussaid, V. G. Chigrinov, *Opt. Express* **18**, 17776 (2010).
- [50] J. K. Gansel, M. Thiel, M. S. Rill, M. Decker, K. Bade, V. Saile, G. von Freymann, S. Linden, M. Wegener, *Science* **325**, 1513 (2009).
- [51] C. Imhof, R. Zengerle, *Optics Commun.* **280**, 213 (2007).
- [52] C. F. Hsieh, R. P. Pan, T. T. Tang, H. L. Chen, C. L. Pan, *Opt. Lett.* **31**, 1112 (2006).
- [53] G. Bruno, M. Losurdo, I. Bergmair, "NIM\_NIL Fabrication of graphene inclusions" in "Nanostructured metamaterials-Exchange between experts in electromagnetics and material science", Studies and reports, Anne F. de Baas ed. Publications Office of the European Union 2009, pp. 88.
- [54] G. Bruno, M. Losurdo, I. Bergmair, "Micro and nanostructuring of graphene using UV-NIL" in Nanostructured metamaterials-Exchange between experts in electromagnetics and material science, Exploitable results, Iris Bergmair ed. Profactor GmbH 2012, pp. 25.
- [55] J. Gao, K. Kempa, M. Giersig, E. M. Akinoglu, B. Han, R. Li, *Adv. Phys.* **65** (6), 553 (2016).
- [56] J. Wang, X. Wang, Z. D. Hu, C. Song, S. Liu, *Optoelectron. Adv. Mat.* **10** (11-12), 847 (2016).
- [57] V. M. Shalaev, *Nat. Photonics* **1**, 41 (2007).
- [58] A. Boltasseva, V. M. Shalaev, *Metamater.* **2**, 1

- (2008).
- [59] N. Yu, F. Capasso, *Nat. Mater.* **13**, 139 (2014).
- [60] S. Sun, Q. He, S. Xiao, Q. Xu, X. Li, L. Zhou, *Nat. Mater.* **11**, 426 (2012).
- [61] L. Huang, X. Chen, H. Mühlenbernd, G. Li, B. Bai, Q. Tan, G. Jin, T. Zentgraf, S. Zhang, *Nano Lett.* **12**, 5750 (2012).
- [62] M. Kang, T. Feng, H. Wang, J. Li, *Opt. Express* **20**(14), 15882 (2012).
- [63] W. Wu, Z. Yu, S. Wang, R. S. Williams, *Appl. Phys. Lett.* 063107 (2007).
- [64] K. A. Bachman, J. J. Peltzer, P. D. Flammer, T. E. Furtak, R. T. Collins, R. E. Hollingsworth, *Opt. Express* **20**(2), 1308 (2012).
- [65] B. M. Ratliff, C. F. LaCasse, J. S. Tyo, *Opt. Express* **17**, 9112 (2009).
- [66] N. Yu, P. Genevet, M. A. Kats, F. Aieta, J. P. Tetienne, F. Capasso, Z. Gaburro, *Science* **334**, 333 (2011).
- [67] K. Yao, Y. Liu, *Nanotechnol. Rev.* **3**, 177 (2014).
- [68] S. Maci, “FORESEEN-Nanoarchitectronics Roadmap”, <https://eledia.science.unitn.it/foreseen>.
- [69] F. Capasso, “MURI Metasurfaces”, [http://projects.iq.harvard.edu/muri\\_metasurfaces/overview](http://projects.iq.harvard.edu/muri_metasurfaces/overview).
- [70] <http://www.gartner.com/newsroom/id/3114217>.
- [71] M. Walker, M. Cryan, P. Strasser, K. Srinivasan, *III-Vs Review* **18**(5), 46 (2005).
- [72] C. M. Soukoulis, *Optics & Photonics News* **17**(6), 16 (2006).
- [73] Z. Liu, H. Lee, Y. Xiong, C. Sun, X. Zang, *Science* **315**, 1686 (2007).
- [74] Z. Liu, S. Durant, H. Lee, Y. Pikus, Y. Xiong, C. Sun, X. Zhang, *Optics Express* **15**(11), 6947 (2007).
- [75] R. D. Averitt, W. J. Padilla, H. T. Chen, J. F. O’Hara, A. J. Taylor, C. Highstrete, M. Lee, J. M. O. Zide, S. R. Bank, A. C. Gossard, *Proc. of SPIE* **6772**, 677209-1 (2007).
- [76] I. V. Shadrivov, A. B. Kozyrev, D. W. Van der Weide, Y. S. Kivshar, *Opt. Express* **16**, 20266 (2008).
- [77] D. A. Powell, I. V. Shadrivov, Y. S. Kivshar, *Opt. Express* **16**, 15185 (2008).
- [78] D. A. Powell, I. V. Shadrivov, Y. S. Kivshar, *Appl. Phys. Lett.* **95**, 084102 (2009).
- [79] J. Henzie, M. Grunwald, A. Widmer-Cooper, P. L. Geissler, P. Yang, *Nat. Mater.* **11**, 131 (2011).
- [80] X. Chen, L. Huang, H. H. Mühlenbernd, G. Li, B. Bai, Q. Tan, G. Jin, C. Qiu, S. Zhang, T. Zentgraf, *Nat. Commun.* **3**, 1198 (2012).
- [81] F. Aieta, P. Genevet, N. Yu, M. A. Kats, Z. Gaburro, F. Capasso, *Nano. Lett.* **12**, 1702 (2012).
- [82] X. Ni, N. K. Emani, A. V. Kildishev, A. Boltasseva, V. M. Shalaev, *Science* **335**, 427 (2012).
- [83] Y. Yao, M. A. Kats, P. Genevet, N. Yu, Y. Song, J. Kong, F. Capasso, *Nano Lett.* **13**, 1257 (2013).
- [84] N. K. Grady, J. E. Heyes, D. R. Chowdhury, Y. Zeng, M. T. Reiten, A. K. Azad, A. J. Taylor, D. A. R. Dalvit, H. T. Chen, *Science* **340**, 1304 (2013).
- [85] J. Y. Ou, E. Plum, J. Zhang, N. I. Zheludev, *Nat. Nanotechnol.* **8**(4), 252 (2013).
- [86] D. Lin, P. Fan, E. Hasman, M. L. Brongersma, *Science* **345**, 298 (2014).
- [87] G. Zheng, H. Mühlenbernd, M. Kenney, G. Li, T. Zentgraf, S. Zhang, *Nat. Nanotechnol.* **10**, 308 (2015).
- [88] M. Inami, D. Sekiguchi, S. Tachi, *Transparent Cloak, Brouchure of Demonstration at Laval Virtual 2003, France* (2003).
- [89] X. Ni, Z. J. Wong, M. Mrejen, Y. Wang, X. Zhang, *Science* **349**, 1310 (2015).
- [90] C. Cotirlan-Simioniuc, A. S. Manea, C. Logofatu, *NIMP Patent Application Request a 2015 00050, RO-BOPI 7, 34* (2016).
- [91] J. Valente, J. Y. Ou, E. Plum, I. J. Youngs, N. I. Zheludev, *Appl. Phys. Lett.* **106**, 111905 (2015).
- [92] L. Li, T. Li, X. M. Tang, S. M. Wang, Q. J. Wang, S. N. Zhu, *Nat. /Light: Sci. & Appl.* **4**, e330 (2015).
- [93] Z. Liu, S. Durant, H. Lee, Y. Pikus, Y. Xiong, C. Sun, X. Zhang, *Opt. Express* **15**, 6947 (2007).
- [94] W. Guo, Z. Li, H. Gao, L. Xia, L. Shi, Q. Deng, C. Du, *Proc. SPIE* **8759**, 87593I-1 (2014).
- [95] Y. Y. Schechner, N. Karpel, *Proc. MTS/IEEE OCEANS*, 1255 (2004).
- [96] M. I. Rusu, C. Pardanaud, C. Martin, Y. Addab, P. Roubin, Y. Ferro, E. Cannuccia, L. Ferry, F. Viot, M. Barrachin, C. P. Lungu, C. Porosnicu, P. Dinca, M. Lungu, M. Köppen, P. Dollase, T. Dittmar, Ch. Linsmeier, *Nuclear Fusion* **57**(7), 076035 (2017).
- [97] A. E. Shabayek, O. Morel, D. Fofi, “Visual Behavior Based Bio-Inspired Polarization Techniques in Computer Vision and Robotics” in *Developing and Applying Biologically-Inspired Vision Systems: Interdisciplinary Concepts*, M. Pomplun, J. Suzuki, eds. IGI Global 2012, pp. 243.
- [98] X. Liu, B. Qiu, Q. Chen, Z. Ni, Y. Jiang, M. Long, L. Gui, *Opt. Express* **22**, 20446 (2014).
- [99] Micronix Plus SRL, [www.termoviziune.ro/ro/Categorii/Sisteme-de-termoviziune-pentru-aplicatii-civile\\_Sisteme-night-vision-pentru-vehicule-105](http://www.termoviziune.ro/ro/Categorii/Sisteme-de-termoviziune-pentru-aplicatii-civile_Sisteme-night-vision-pentru-vehicule-105).
- [100] A. J. Yuffa, K. P. Gurton, G. Videen, *Appl. Opt.* **53**, 8514 (2014).
- [101] Pike Technologies Catalog, “FTIR and UV-Vis Accessories and Supplies” (2013).
- [102] S. Larouche, Y. Tsai, T. Tyler, N. M. Jokerst, D. R. Smith, *Nat. Mater.* **11**, 450 (2012).
- [103] V. Sankaran, M. J. Everett, D. J. Maitland, J. T. Walsh, Jr., *Opt. Lett.* **24**, 1044 (1999).
- [104] T. Novikova, A. Pierangelo, A. De Martino, A. Benali, P. Validire, *Opt. Photonics News* **23**, 26 (2012).
- [105] H. Y. Shen, P. C. Zhou, S. R. Feng, *Proc. SPIE* **8193**, 81930M (2011).
- [106] T. R. Jensen, M. D. Malinsky, C. L. Haynes, R. P. Van Duyne, *J. Phys. Chem. B* **104**, 10549 (2000).